A dynamic ammonia emission model and the online coupling with WRF-Chem (WRF-SoilN-Chem v1.0): development and evaluation

Chuanhua Ren[1], Xin Huang[1,2], Tengyu Liu[1,2], Yu Song[3], Zhang Wen[4], Xuejun Liu[4], Aijun Ding[1,2], Tong Zhu[3]

[1] School of Atmospheric Sciences, Nanjing University, Nanjing, China
[2] Jiangsu Provincial Collaborative Innovation Center for Climate Change, Nanjing, China
[3] College of Environmental Sciences and Engineering, Peking University, Beijing, China
[4] College of Resources and Environmental Sciences, China Agricultural University, Beijing, China

Correspondence to: Xin Huang (xinhuang@nju.edu.cn)

Abstract.

Volatilization of ammonia (NH_3) from fertilizer application and livestock wastes is an overwhelmingly important pathway of nitrogen losses in agricultural ecosystems and constitutes the largest source of atmospheric NH_3. The volatilization of NH_3 highly depends on environmental and meteorological conditions, however, this phenomenon is poorly described in current emission inventory and atmospheric models. Here, we develop a dynamic NH_3 emission model capable of calculating NH_3 emission rate interactively with time- and spatial-varying meteorological and soil conditions. The NH_3 flux parameterization relies on several meteorological factors and anthropogenic activity including fertilizer application, livestock waste, traffic, residential and industrial sectors. The model is then embedded into a regional WRF-Chem model and is evaluated against field measurements of NH_3 concentrations and emission flux, and satellite retrievals of column loading. The evaluation shows a substantial improvement in the model performance of NH_3 flux and ambient concentration in China. The model well represents the spatial and temporal variations of ambient NH_3 concentration, indicating the highest emission in the North China Plain (NCP) and Sichuan Basin, especially during summertime. Compared with normal simulations using fixed emission inventory input, this model features superior capability in simulating NH_3 emission flux and concentration during drastic weather changes like frontal activities and precipitation. Such advances in emission quantification also improve the model performance of secondary inorganic aerosol on synoptic scales. While more laboratory and field measurements are still needed for better parameterization of NH_3 volatilization, the seamless coupling of soil emission with meteorology provides a better understanding of NH_3 emission evolution and its contribution to atmospheric chemistry.

1 Introduction

Ammonia (NH_3) is the most important alkaline gas in the atmosphere and has important impacts on the ecological environment and human health (Behera et al., 2013). Gas-phase NH_3 can react with ambient sulfuric and nitric acids to form ammonium sulfate (($NH_4)_2SO_4$), ammonium bisulfate (NH_4HSO_4) and ammonium nitrate (NH_4NO_3) aerosols (Wang et al., 2013), which

constitute a significant fraction of atmospheric fine particles associated with potential human health impacts (Emmanouil et al., 2017; Oprea et al., 2017). Besides, soil NH_3 volatilization releases a large amount of nitrogen into the atmosphere, which

35 is in turn deposited back to terrestrial and aquatic ecosystems, contributing to acid deposition and eutrophication. Thus, the atmospheric emission, transport and deposition of NH_3 play a societally and ecologically important role in the global nitrogen cycle (Fowler et al., 2013; Liu et al., 2022).

Due to the health and ecological significance of atmospheric NH_3, a range of air quality models have been applied to investigate its spatiotemporal variation and sink (Spindler et al., 2001; Asman, 2001; Van Pul et al., 2009). To accurately

40 simulate NH_3 in numerical models, considerable approaches have been developed to estimate NH_3 emissions from natural and anthropogenic sources, which vary greatly in their complexity and data requirements. A common method named "Bottom-up" method is to use emission factors multiplied by activity data (e.g., fertilizer application amounts corresponding to each crop, mileage of motor vehicles, etc.). Based on this approach, several organizations and researchers established gridded NH_3 emission inventories, such as the MEIC, PKU-NH_3, EDGAR, and REAS (Li et al., 2017; Huang et al., 2012; Paulot et al.,

45 2014; Crippa et al., 2020; Kurokawa and Ohara, 2020). Based on the human activity level and land-use type in different regions, the bottom-up emission inventories can reflect geographic variations. In addition, these inventories offer highly formatting gridded dataset of monthly variation and spatial distribution of NH_3 emission, which are extensively utilized in atmospheric chemical transport models.

On both global and regional scales, NH_3 is mostly emitted from agricultural activities, mainly including the fertilization and

50 livestock waste (Bouwman et al., 1997). Multiple lines of evidence from field trials, meta-analysis, and a statistical model indeed showed that local meteorological conditions strongly influence ammonia emission rate (Paerl, 2002; Misselbrook et al., 2005; Bouwman et al., 2002). Temperature is the most important meteorological parameter that affects the partial pressure of NH_3 in soil by changing the equilibrium constant of the NH_4^+(soil)-NH_3(soil)-NH_3(gas) equilibrium reaction (Van Slyke and Cullen, 1914; Clay et al., 1990). Furthermore, high temperature increases the rate of urea hydrolysis and the diffusion rate of

55 NH_4^+ and NH_3 in soil (Overrein and Moe, 1967). Riddick et al. (2016) showed that increasing the ground temperature from 290 to 300 K (at a pH of 7) increases the NH_3 emissions by a factor of 3. Besides temperature, soil moisture also strongly controls NH_3 loss by influencing urea hydrolysis and NH_3/NH_4^+ concentration in soil solution. Results from a field experiment showed that the rate of ammonia volatilization was highly limited at low soil moisture even though the ammoniacal N concentration and pH were high (Smith et al., 1988). On the contrary, if the soil moisture content is quite high, the concentration

60 of ammonia in solution tends to be diluted and thus the ammonia volatilization is prone to be reduced (Fenn and Kissel, 1976). Moderate amounts of soil moisture are found to be more favourable for NH_3 volatilization. Additionally, rainfall, wind speed and RH have also been proved by laboratory experiment to affect NH_3 emissions (Longhini et al., 2020; Parker et al., 2005). Generally, the environment elements appreciably influencing ammonia emissions have drastic weather-scale variations or diurnal variations. As one of the main monsoon regions, with the most intense agriculture activities in the world, east Asia is

65 a region experiencing complex synoptic weather and high-level NH_3 emission (Ding et al., 2017; Van Damme et al., 2015; Zhang et al., 2017). Dramatic changes of ammonia emissions caused by different meteorological conditions could also

substantially influence the level of nitrogen-containing aerosol (e.g. ammonium nitrate) at the same time. However, the majority of current temporal resolution of existing ammonia inventory still remains at the monthly or annual scale, which is not capable of accurately reflecting the time-resolved and spatial-varying ammonia emission due to weather change on synoptic

70   scale.

Although in recent years, bidirectional flux models that consider the meteorological influence have been applied in regional chemistry models (Cooter et al., 2010; Zhang et al., 2010a), such as the WRF-CMAQ-EPIC model (Pleim et al., 2019), this method requires users to collect and build complex agriculture-related files. In this work, we develop and evaluate a new user-friendly ammonia flux module (WRF-SoilN-Chem) capable of simulating dynamic NH_3 volatilization under different

75   meteorological conditions. The whole NH_3 flux model and input dataset are embedded directly into the WRF-Chem model and can be activated by simply turning on an option in the model control file. It then enables the seamless coupling of meteorology simulation, the NH_3 flux flows and atmospheric chemistry module. The WRF-SoilN-Chem model is easy to install and use, open source, version controlled and well documented. In this paper, section 2 presents the overall methodology including a detailed description of the model's framework, data source and emission factor algorithm. Section 3 compares the

80   simulated NH_3 flux and concentrations with site measurements and satellite retrievals, and in-depth analyses of case studies where the simulation of ammonia and secondary inorganic aerosol are improved on a synoptic scale. Further discussion of the dynamic model like bidirectional parameterization and other dynamic reactive nitrogen emission models are provided in section 4.

2 Materials and methods

85   ### 2.1 The parent model: WRF-Chem

WRF-Chem is a state-of-art online coupled meteorology-chemistry model that can simulate meteorological fields and atmospheric chemical compositions including aerosols (Grell et al., 2005). It has been widely used in air quality forecasting and aerosol-related studies (Chen et al., 2016). WRF model provides users with many options for model configurations and physical schemes, and is used to simulate meteorological processes and advection of atmospheric constituents. WRF uses the

90   Advanced Research WRF (ARW) dynamical solver, which solves fully compressible, Eulerian non-hydrostatic equations on either hybrid sigma–eta (default) or terrain-following vertical coordinates defined by the user. Besides, the WRF model offers many options for land surface physics, planetary boundary layer physics, radiative transfer, cloud microphysics, and cumulus parameterization, for use in meteorological studies, real-time numerical weather prediction, idealized simulations, and data assimilation on meso- to regional scales (Skamarock, 2019). WRF-Chem is an extended version of WRF including atmospheric

95   chemistry and aerosols. The chemical transport model numerically solves the concentration of chemical species through emissions, advection, vertical mixing with dry deposition, convective transport, gas chemistry, cloud chemistry (for activated aerosols in cloud water), aerosol chemistry, and wet scavenging. WRF-Chem can simulate trace gases and particles in an

interactive way, allowing for feedbacks between the meteorology and radiatively active gases and particles. The detailed model configuration is described in Sect. 3.1.

2.2 General framework of Model WRF-SoilN-Chem

The dynamic NH_3 flux model within WRF-Chem model estimates the emission rate of NH_3 (mol m^{-2} hour^{-1}) from the natural and anthropogenic source into the atmosphere at a specific location and time. Figure 1 gives an architectural overview of the WRF-SoilN-Chem coupled model. Briefly, the model contains three parts: (1) the static input data, (2) the WRF mesoscale meteorological model, (3) and online NH_3 emission model coupled into Chem model. The static input data cover the whole China region with ~1 km^2 spatial resolution. The emission sources are classified into six sectors, including fertilizer application, livestock waste, agriculture soil, transport, residential and industrial sectors. The data are embedded into *geog_data_path* as binary format and read by *geogrid.exe* in WPS. The WRF model is used to set up the simulation initialization and perform dynamical and physical calculations. The online NH_3 model is merged into Chem module by modifying the *chem_driver* and *emissions_driver* modules.

Users can turn on the dynamic NH_3 emission model in WRF-Chem by specifying *nh₃emis_opt = 1* in *namelist.input* control file, similar to the way that users specify the dust emission mechanism in WRF-Chem. The simulated environmental conditions like meteorological element and soil properties provided by WRF solver are transported to NH_3 emission model to calculate the meteorology-dependant emission factor (EF). Consequently, the EF is multiplied by the part (1) static input data to obtain NH_3 flux and the NH_3 flux flows to Chem model to participate in the chemistry routine (deposition, computation, convection, boundary layer mixing, and chemistry). At the end of the WRF-SoilN-Chem simulation, WRF outputs all meteorological, NH_3 emission rates and other chemical diagnostic quantities in WRF's standard format.
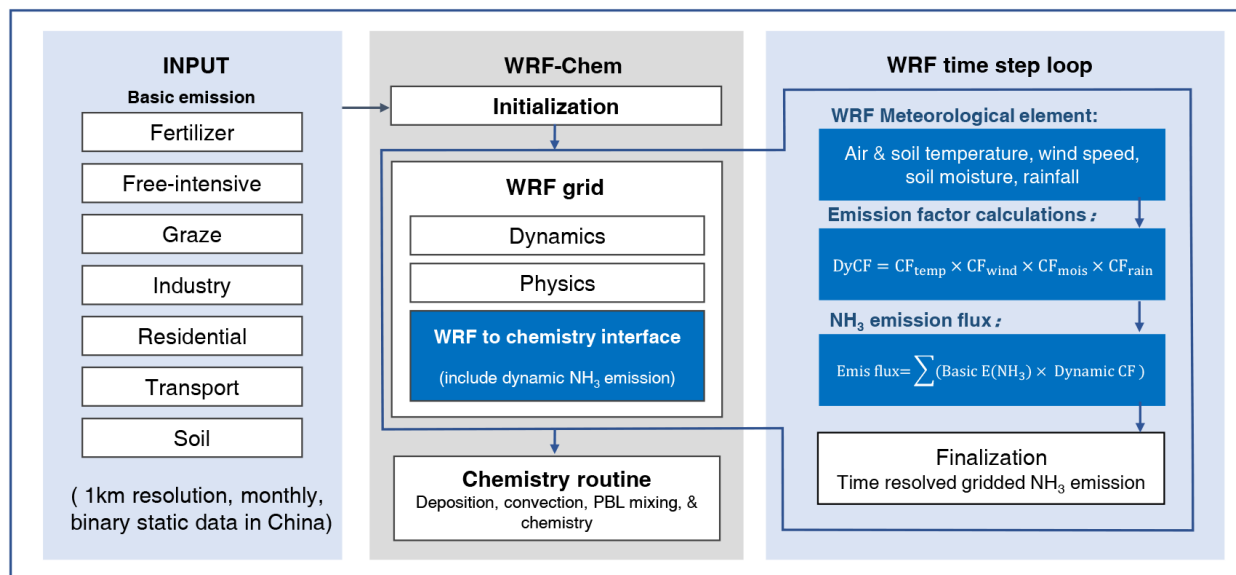
Figure 1: Architectural overview of the WRF-SoilN-Chem model (v1.0). The NH₃ emission flux calculation (all parts shown in blue) includes basic emission data and dynamic calculation. The parent model (shown in grey) are standard codes downloaded from their sources, without any modification.

2.3 Basic emission data

In this study, the basic emission data were divided into six sections which are fertilizer application, livestock waste, agriculture soil, transport, residential and industry, covering a total of more than 50 emission sources. Due to intensive agriculture activities in China, synthetic fertilizer application and livestock manure represent the most important sources of NH₃, jointly accounting for more than 80−90 % of total emissions in China (Li et al., 2021). In fertilizer section of basic emission, urea and ammonium bicarbonate (ABC) are two dominant emitters, followed by others like ammonium nitrate and ammonium sulfate. For the livestock waste section, nitrogen in animal excrement in the form of urea can rapidly hydrolyze to form ammonium carbonate and then volatilize as gaseous NH₃. The other minor sources include agricultural soil, N-fixing plants, the compost of crop residues, biomass burning, excrement waste from rural populations and chemical industry, waste disposal, traffic sources and NH₃ escape from thermal power plants. All the basic static emissions data were calculated as a product of the activity data and corresponding static EFs, as shown in equation (1):

$$Basic\ E(NH_3) = \sum_i \sum_p \sum_m (A_{i,p,m} \times EF_{static\,i,p,m}) \qquad (1)$$

where $Basic\ E_{(NH_3)}$ is the basic NH₃ emissions of a specific source section; i, p, and m represent source type, the province of China, and the month, respectively. $A_{i,p,m}$ is the activity data of a specific source; and $EF_{static\,i,p,m}$ is the reference emission factor for static conditions.

In the fertilizer application section, soil pH and fertilizer application rate and method are relatively stable in a short time, thus they were introduced as stabile parameters to adjust emission factors for static conditions. The static EF of fertilizer is shown

140   in equation (2):

$$EF_{static_{fertilizer}} = EF_{0i} \times CF_{pH} \times CF_{method} \times CF_{rate} \tag{2}$$

where EF_{0i} is the reference emission factor for a type i fertilizer. CF_{pH} is the correction factor for different soil acidity. CF_{method} is the correction factor for the fertilization method, including basal dressing and top dressing. CF_{rate} is the correction factor for different application rates.

145   As for the livestock waste section, free-range, grazing and intensive are three main animal-rearing system in China and produce a huge number of wastes. The NH_3 emissions can be converted into gaseous NH_3 or lost through other pathways during different processes of manure management, including animal housing, manure storage, manure spreading and the grazing stage (Webb and Misselbrook, 2004; Webb et al., 2006). The ammonia emissions from each stage of livestock manure management are affected by many factors, such as species, age, housing structure, manure storage system, spreading technique, time spent

150   outside or inside and meteorological conditions (Zhang et al., 2010b). In the livestock section, the static emission factors are set separately according to the animal species, age, manure status and rearing system, as shown in equation (3):

$$EF_{static_{livestock}} = EF_{c,a,s,f} \tag{3}$$

where $EF_{c,a,m,f}$ represents the emission factor of livestock waste, c represents each animal classes, a represents different age, s represents different rearing system, such as grazing, free-range and intensive, and f represents the form of manures like

155   slurry or solid manures.

As for other miscellaneous sources, further details on the estimation methods and gridded and monthly allocation of the various sources are fully presented in Huang et al. (2012). All the basic emissions are allocated to each 1 km spatial resolution on the basis of land cover, rural population, and other proxies. Eventually, the data is converted to the binary format and embedded into *geog_data_path* required by WPS.

160   **2.4 Meteorology-dependant NH₃ dynamic emission factor**

In this section, we describe the algorithm for dynamic ammonia emissions from fertilizer application and livestock waste. For fertilizer application, the main factors governing ammonia volatilization are identified to be ammoniacal N concentration, soil pH, temperature in soil or floodwater, wind speed, soil moisture and rainfall by a variety of lab-experiments. In this study, ammoniacal N concentration and soil pH are relatively stable in short term and are represented by monthly activity data like

165   fertilizer N application and CF_{pH} respectively. However, other factors that change dynamically under different meteorological conditions need to be calculated in real time in the model. The effects of these dynamical factors on ammonia emissions are reflected by the following correction factors, and the calculations are performed in WRF-Chem model at each time step. The dynamic NH₃ emission flux from fertilizer is estimated using Eq. (4):

$$Flux_{NH3-fertilizer} = Basic\ E(NH_3)_{fertilizer} \times CF_{wind} \times CF_{soil_T} \times CF_{soil_m} \times CF_{rain} \tag{4}$$

170 where $Basic\ E(NH_3)_{fertilizer}$ represents the base emission presented on Sect. 2.3. CF_{wind} is the correction factor for wind

speed; and CF_{soil_T} is the correction factor for soil temperature; CF_{soil_m} is the correction factor for soil moisture content; CF_{rain}

is the correction factor for rainfall. The detailed calculation of these CFs is presented in the following sub sections, and Table

1 summarizes the relevant variables used in WRF-SoilN-Chem. Ammonia emissions could then be calculated as the product

of monthly basic emissions and corresponding condition-specific correction factors.

175 For livestock waste, we divided the NH₃ emissions into three sections based on where the manure was located, including

manure storage, outdoor and housing. Estimations were made by multiplying the basic source data by the corresponding CFs.

As for the manure storage section, the handle practice of excrement is usually settled in closed containers at artificially set

temperatures for biogas generation and composting. This part of NH₃ emissions is not affected by the outdoor environment

and therefore does not need to be corrected.

180 For outdoor farming such as grazing and free range and the application of manure into a field, the excreta were directly

deposited in the open air without any treatment. Since the emissions are directly affected by local atmospheric conditions, the

estimation of outdoor emission is the same as above for fertilization.

$$Flux_{NH3-hus-outdoor} = Basic\ (E_{outdoor}) \times CF_{wind} \times CF_{soil_T} \times CF_{soil_m} \times CF_{rain} \qquad (5)$$

where $Basic\ (E_{outdoor})$ represents the basic emission from outdoor livestock waste, including outdoor grazing in daytime,

185 outdoor free-ranging and manure spreading onto field.

For the housing section, since animals are farmed in buildings, NH₃ emissions are directly affected by indoor temperature and

ventilation rate. To maintain a healthy environment inside the animal houses a suitable ventilation rate and temperature are

required. Specifically, when the outside temperatures drop below a certain level, farmers usually install manual heating to

maintain stable temperatures to prevent the decline of animal production. When the outside temperature reaches a maximum

190 level, the mechanical ventilation system is opened to maintain the temperature inside the animal house close to the

recommended temperature (Gyldenkaerne et al., 2005).

$$Flux_{NH3-hus-house} = Basic\ (E_{house}) \times CF_{houseV} \times CF_{houseT} \times CF_{soil_m} \qquad (6)$$

where $Basic\ (E_{house})$ represents the basic emission from animal houses, including indoor grazing at night, and intensive

rearing. The indoor wind speed and temperature are calculated according to outdoor weather conditions, and the detailed

195 calculation methods were reported by (Gyldenkaerne et al., 2005).

2.4.1 Wind speed

Increasing wind speed increases the rate of ammonia volatilization by promoting the rapid transport of ammonia away from

the surface. Denmead et al. (1982) suggested that the enhanced volatilization at higher wind speeds is due to better mechanical

mixing of the N solution in the soil, which replenishes ammonia in the layer next to the surface. And Denmead et al. (1982)

200 found an exponential relationship between the transfer velocity for ammonia and wind speed. After testing and comparing

several published approaches, we followed the approach of Gyldenkaerne et al. (2005) to introduce the effects of wind speed on NH_3 volatilization from synthetic fertilizer and manure application. The correction factor of wind speed is:

$$CF_{wind} = e^{(0.0419 \times WS)} \tag{7}$$

where WS is the surface wind speed (m s^{-1}).

2.4.2 Soil temperature

Temperature is the most important meteorological parameter that affects the partial pressure of NH_3 in soil by changing the equilibrium constant of the NH_4^+(soil)-NH_3(soil)-NH_3(gas) equilibrium reaction. Several studies have noted an increase in emission from N fertilizers and livestock waste with increasing temperature, and revealed the empirical volatilization rates as functions of air temperatures (Sommer et al., 1991; Pedersen et al., 2021). Mcinnes et al. (1986) reported that diurnal patterns of NH_3 loss coincided with fluctuations in soil temperature and water content. However, after our tests, we found that the published relationship can hardly reflect the diurnal pattern of the ammonia flux. Thus, the effects of soil temperature and in situ measurements of NH_3 flux conducted by our research group in a typical cropland were involved to further refine the CF for synthetic fertilizer and manure emissions in this study. The exponential fitting of CF_{soil_T} is:

$$CF_{soil_T} = e^{(0.093 \times \Delta soil_T - 0.97 + 0.018 \times soil_T)} \tag{8}$$

where $\Delta soil_T$ is the soil temperature gradient, and it can be represented by the difference between the soil temperature of 5 cm and surface skin temperature (K); $soil_T$ is the soil temperature (K) at the depth of 5 cm.

2.4.3 Soil water

The soil moisture content is also an important factor controlling ammonia loss. The presence of water in soil is a prerequisite for dissolution of fertilizer N as well as for the hydrolysis of urea, leading to the conversion of other forms N to ammoniacal N in soil solution. Ammonia volatilization can also be enhanced where water evaporates from the soil surface. On the other hand, if the soil moisture content is high, the concentration of NH_4^+ in solution will be low due to dilution and NH_3 volatilization should be reduced. Ferguson and Kissel (1986) and Fenn and Kissel (1976) also found that ammonia loss was low when soil moisture was at the extremes. Experiments from Maru et al. (2019) showed that the moderate amounts of soil moisture content were around 50 %, where the NH_3 emission reached a peak at this turning point (Maru et al., 2019). Considering the complex effect of soil moisture, we followed the approach of Lian et al. (2021) to introduce the two kinds of effects on NH_3 volatilization. The correction factor of soil moisture is:

$$CF_{soil_m} = \begin{cases} 0.45 \times e^{(-1 \times soil_m)} + 0.55 & if \ soil_m \geq 0.5 \\ 0.49 \times e^{soil_m} & if \ soil_m < 0.5 \end{cases} \tag{9}$$

where $soil_m$ represents the soil water content (m^3 m^{-3}) at the depth of 5 cm.

2.4.4 Rain fall

230   Several studies reported that rainfall events after fertilizer application can influence the maximum potential emission of NH_3 in the field (Parker et al., 2005; Smith et al., 2009). Wind tunnel experiments from Sanz-Cobena et al. (2011) showed that the addition of 7 and 14 mm of water to the soil, immediately after urea fertilizing, reduced NH_3 emission by 77 % and 89 %, respectively. We derived a relationship between emission rate and rainfall for agriculture emissions based on the available native experimental data (Longhini et al., 2020). The correction factor of rainfall is:

235   $CF_{rain} = 1/(3.2 \times rainfall + 1)$

where $rainfall$ is the precipitation (mm hr^{-1}) simulated from the WRF model.

Table 1. Meteorological and activity variables required to drive WRF-SoilN-Chem

No.	Variables in WRF-SoilN-Chem [units]	Description	Usage
1.	AGRISOIL [kg km^{-2} month^{-1}]	Soil emission	Basic emission
2.	FERTILIZER [kg km^{-2} month^{-1}]	Fertilizer emission	Basic emission
3.	FREE-INTEN [kg km^{-2} month^{-1}]	Free range & intensive emission	Basic emission
4.	GRAZE [kg km^{-2} month^{-1}]	Grazing emission	Basic emission
5.	INDUSTRY [kg km^{-2} month^{-1}]	Industry emission	Basic emission
6.	RESIDENTIAL [kg km^{-2} month^{-1}]	Residential emission	Basic emission
7.	TRANSPORT [kg km^{-2} month^{-1}]	Transport emission	Basic emission
8.	EFnh3 [unitless]	Dynamic EF	Met-dependent factor
9.	U10 [m s^{-1}]	East-west wind at 10m height	Wind factor
10.	V10 [m s^{-1}]	North-south wind at 10m height	Wind factor
11.	T2 [K]	Surface temperature	Temperature factor
12.	TSK [K]	Surface skin temperature	Temperature factor
13.	TSLB [K]	Soil temperature	Temperature factor
14.	SMOIS [m^3 m^{-3}]	Soil moisture	Soil water factor
15.	RAINNC [mm hr^{-1}]	Accumulated total grid scale precipitation	Rainfall factor
16.	T_house	Indoor temperature	Temperature factor
17.	V_house	Indoor ventilation rate	Wind factor
18.	freq_residential [unitless]	Residential diurnal pattern	Activity time
19.	freq_industry [unitless]	Industry diurnal pattern	Activity time
20.	freq_transport [unitless]	Transport diurnal pattern	Activity time

21.	rho_phy [kg m^{-3}]	the air density	Unit conversion
22.	dtstep [s]	the meteorology big time step in seconds	Time loop
23.	dz8w [m]	the vertical grid spacing for the lowest layer	Unit conversion
24.	emis_ant [mol km^{-2} hr^{-1}]	Anthro emission rate	Total emission
25.	current_hour	Emission time	Time

3 Evaluation

3.1 Modelling configuration for estimating China's ammonia emission

To evaluate the dynamic NH$_3$ flux model and figure out the aerosol response to dynamic NH$_3$ emission, we designed a pair of parallel experiments in WRF-Chem . The simulation with the coupled dynamic model is referred to as the "*online*" experiment, while the simulation without the dynamic model is referred to as "*base*" experiment. The base simulation used monthly country-level NH$_3$ inventory based on PKU-NH$_3$ inventory, which is described by Huang et al. (2012). Other anthropogenic gas emissions from power plant, industrial, residential, and vehicle sectors were taken from the MEIC database (Li et al., 2017). Both two experiments were run for the entire year of 2019 over the NH$_3$ hot-spot region in eastern China (18° N–50° N, 95° E–131° E) with 20 km grid resolution. The main configurations for the two experiments are listed in Table 2. A new version of the rapid radiative transfer model for general circulation model applications (RRTMG) was employed to depict the radiative transfer process for both shortwave and longwave radiation (Iacono et al., 2008). The Noah land surface scheme (Ek et al., 2003) was used to describe the land–atmosphere interactions, implemented with the Yonsei University PBL scheme (Hong et al., 2006) to describe the diurnal evolution of the planet boundary layer (PBL). As for cloud and precipitation processes, the new Grell–Freitas cumulus ensemble parameterization (Grell and Freitas, 2014) along with Lin microphysics (Lin et al., 1983) accounting for six forms of hydrometers were employed. The WRF simulation was thoroughly evaluated through comparison to comprehensive surface meteorology data and compiled in a publicly accessible report (U.S. EPA, 2021). As for Chem model, the Model for Simulating Aerosol Interactions and Chemistry (MOSAIC) (Zaveri et al., 2008) and the CBM-Z (carbon bond mechanism) photochemical mechanism (Zaveri and Peters, 1999) were used. The MOSAIC aerosol scheme includes physical and chemical processes of nucleation, condensation, coagulation, aqueous phase chemistry, and water uptake by aerosols.

Table 2. WRF-Chem domain setting and configuration selection

Domain setting	
Simulation region	18°N–50°N, 95°E–131°E
Grid spacing	20 km × 20 km
Vertical layers	29
Map projection	Lambert conformal

Configuration selections	
Land surface	Noah
Boundary layer	YSU
Microphysics	Lin et al.
Cumulus	Grell-Freitas
Radiation	RRTMG
Chemistry	CBMZ
Aerosol	MOSAIC

260

3.2 Spatiotemporal pattern of ammonia emission in China

In 2019, the total atmospheric ammonia emission in China was estimated to be 12.67 Tg, and the emission density was around 1.32 Mg km^{-2}. The total amount was approximately threefold that obtained for Europe (4.18 Tg) and contributed approximately 38 % of Asian NH$_3$ emissions (Kurokawa and Ohara, 2020). Further, this estimated emission was relatively close to the

265 improved emissions based on AMoN-China and the ensemble Kalman filter (13.1 Tg) (Kong et al., 2019). The most important contributor is livestock manure management (5.25 Tg), accounting for approximately 41.4 % of the total budget. Next is the fertilizer application (5.09 Tg), which was responsible for 40.1 % of emissions. With high nitrogen content of about 46 %, urea fertilizer is the most widely used N fertilizer in China, accounting for 89 % of the total fertilizer. Regarding livestock waste, the free-range is the largest contributors (65.6 %) to livestock-waste-related NH$_3$ emissions. Next is intensive rearing

270 (approximately 30 %), which refers to the process of raising livestock in confinement at high stocking density; in this process, the farm operates as a factory. Grazing, a relatively less important system without additional feed supplementation, only dominates in the northern and western parts of China.
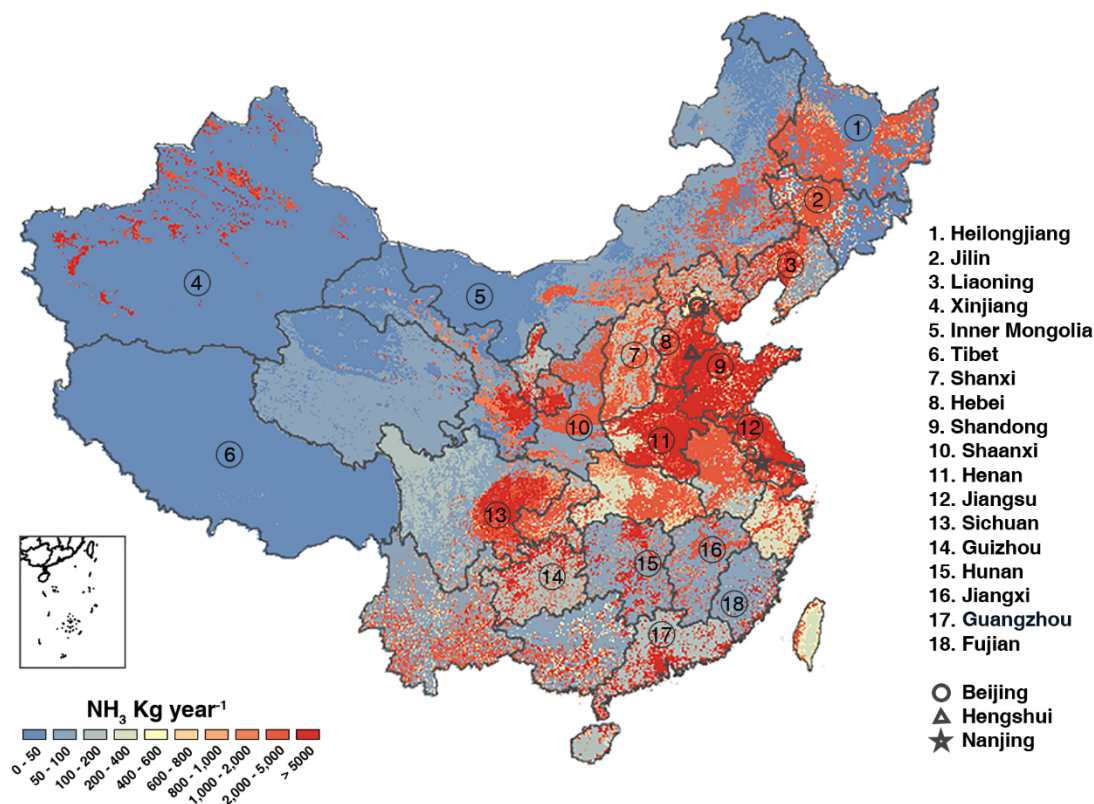
Figure 2: Spatial distribution of basic ammonia emissions in 1 km grid cell (kg yr^{-1}).

275

The spatial distribution of NH$_3$ emissions in 2019 is illustrated in Fig. 2. It is clear that the high emission rate concentrates in Shandong, Jiangsu, Henan and Hebei provinces and in eastern Sichuan. Shandong province has the highest NH$_3$ emission density of 4.46 Mg km^{-2}, which is 3 times higher than the national average. Multiple-cropping system is a wildly applied agricultural practice in China and varies from region to region. North-eastern China is a mainly single-cropping area, with spring wheat as the main crop. The double-cropping area (~27.74 % of total cropland area) is mainly distributed in the North

280 China Plain (NCP), with a 25,624,000 and 5,754,000 ha area under cultivation of cereal crops and vegetables, respectively, is responsible for 49 % of the NH$_3$ emissions from fertilization in China. Triple-cropping and limited triple-cropping systems are prevalent in southern China due to the tropical subtropical monsoon climate with high temperature and ample rainfall. With intensive cultivation, the cropping land in Guangdong, Fujian, Hunan and Jiangxi provinces also shows large NH$_3$

285 volatilization. Paddy fields are common in this region, with early rice and late rice being the dominant crop and contributing the most emissions. The smaller emitters are located mostly in western China, with a minimal amount of arable land or low use of synthetic nitrogenous fertilizers.

The spatial distribution of NH₃ emissions from livestock waste is similar to that from synthetic fertilizers, with high emission rates in NCP, eastern Sichuan, and western parts of Xinjiang province. Besides intensive agriculture fertilization, Henan, Shandong, Hebei and eastern Sichuan provinces are well-known for their large animal population. In Henan, Hebei and Shandong, many kinds of animals are extensively bred like beef, dairy, pork and poultry, providing approximately 0.38 Tg, 0.31 Tg and 0.48 Tg ammonia emissions, respectively. Sichuan province is also a large emitter (0.30 Tg), with cattle and pig as the main animals accounting for most emissions. In Tibet and Xinjiang provinces, sheep are widely raised, which is responsible for remarkable ammonia emissions related to sheep manure management. Cattle are widely raised in northeast China and are responsible for around 50 % of the NH₃ emission in Liaoning and Heilongjiang provinces.

The peak of NH₃ emission over NCP might be the joint result of intensive agricultural activities and environmental conditions like high soil pH and wind speed. In China, the soils in the NCP are mainly neutral (pH 6.5−7.5) or alkaline (pH >7.5), and soils distributed in southern or northeastern China are mainly acid soil (pH 5.5−6.5) or strong acid soil (pH < 5.5). NH₃ volatilization increases significantly with an increase in soil pH, due to the high potential for NH₃ emission (Ryan et al., 1981). Thus, the relatively high pH in northern China is another key reason for the large flux in the NCP. Besides soil acidity, NH₃ volatilization increases exponentially with wind speed. Spatially, northern China features frequent strong wind. The annual mean wind speed varied from 4.64 m s⁻¹ north-eastern China to 3.55 m s⁻¹ southern China (Liu et al., 2019). Higher wind speed leads to rapid NH₃ release from soil to the atmosphere, which may contribute to the high ammonia emissions in the northern part of China.

In addition to great regional disparities, China's NH₃ emission is also characterized by obvious seasonality. The monthly variation in Fig. 3 clearly indicates that the emissions were primarily concentrated from April to September due to the intensive agricultural activities and high temperature. In China, the new spring seeding generally begins in April. During this period, spring wheat, soybeans and cotton are sown in the single-cropping area with a large amount of N fertilizer applied to the cropland as the base fertilizer. In the following 1–2 months, due to the application of top fertilizer and warming air temperature, NH₃ emissions tend to continuously increase to August. From summer on, the winter wheat–summer maize rotation system begins in the NCP. The winter wheat–summer maize rotation system has been practiced as a characteristic farming practice, producing about 60 % of the total wheat and 33 % of the total maize production in China (Zheng et al., 2021). There are two cropping cycles for the NCP region beginning in summer and late-autumn, respectively. June to August is one of the main cropping periods in the NCP, with the sowing, basal dressing and top dressing of summer maize. The seeding and basal dressing of winter wheat begin in mid-September and the top dressing is applied 2 months later, which could be responsible for the high emission rate during the autumn season. Meanwhile, in southern China with a large triple-cropping area, fertilization of early and late rice was carried out intermittently from April to mid-October. Most of the crops begin to harvest in the autumn, which lead to a declining emission since then. Different from the hot seasons, because of the less NH₃ volatilization related to lower temperatures and relatively rare cultivation during the winter, the NH₃ emissions decreased to one-third of summer levels.

Figure 3 also shows that the monthly national average NH$_3$ emission in China features obvious day-to-day variation with large disparities between 10th and 90th percentiles, especially during hot seasons. Such a large discrepancy in daily emission rate could be attributed to the highly fluctuating daily weather condition and the associated meteorological parameters throughout the year, and the existence of the summer monsoon makes China have more obvious daily emission changes in summer.

325   However, the fixed NH$_3$ emission inventories that are wildly utilized currently assume no daily variation of emission rate, and thus could not represent the day-to-day variation of emission rate under real weather conditions.
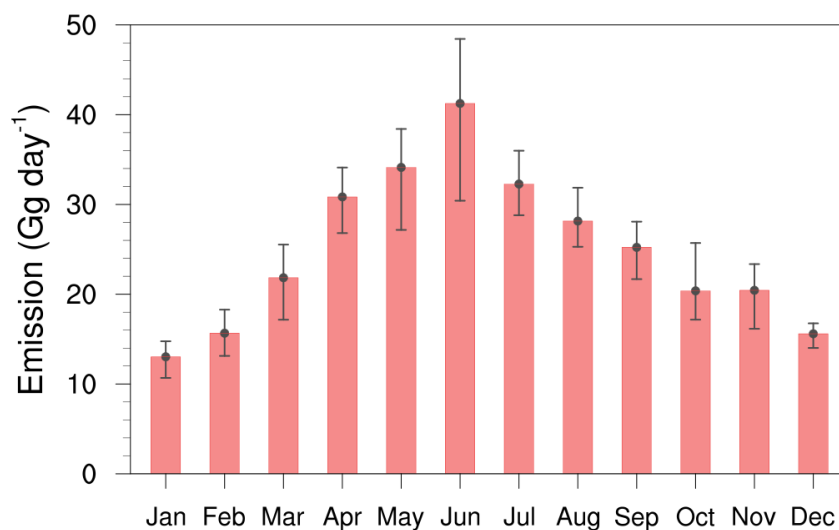
Figure 3: Seasonal pattern of averaged daily ammonia emission in eastern China (18°N–50°N, 95°E–131°E). The lower and upper points of vertical lines show the 10th and 90th percentiles, respectively.

330

3.3 Evaluation of spatiotemporal pattern by monitoring network and satellite retrievals

To better validate the model performance on the spatial and temporal pattern of NH$_3$ emission, we then collected NH$_3$ concentration measurements across China and compared them with the corresponding result from WRF-SoilN-Chem model. Ideally, the model results and observed data should be in the same period in 2019. However, NH$_3$ is not routinely measured at

335   national networks, so there is a lack of published observations for the last five years in China. Since the main emission source of atmospheric NH$_3$ and the activity level would not vary a lot in a short time, therefore, a database of atmospheric nitrogen concentration from the nationwide monitoring network (NNDMN) between 2010 to 2015 is used to evaluate the spatial pattern and magnitude of surface NH$_3$ concentrations in China (Xu et al., 2019). Figure 4 shows spatial plots of annual observed NH$_3$ by NNDMN and two sets of model results. In Fig. 4(a), the base experiment underestimated NH$_3$ concentration in areas with

340   a high emission density. For instance, the NH$_3$ concentrations in sites located in the southern region of Hebei province and the north of Shandong province were underestimated by ~15 ppb. Besides, the base experiment cannot reproduce the high level of NH$_3$ in the Pearl River Delta region (PRD). Nonetheless, in southern China, the base experiments overestimated NH$_3$

concentration by ~5 ppb for the two northern sites in Hubei province. In Fig. 4(b), the spatial accuracy of online experiment is better than that of the base fixed inventory. The online model well reproduces the overall pattern of high values in the NCP,

345 the Sichuan Basin and PRD and low values in other regions.
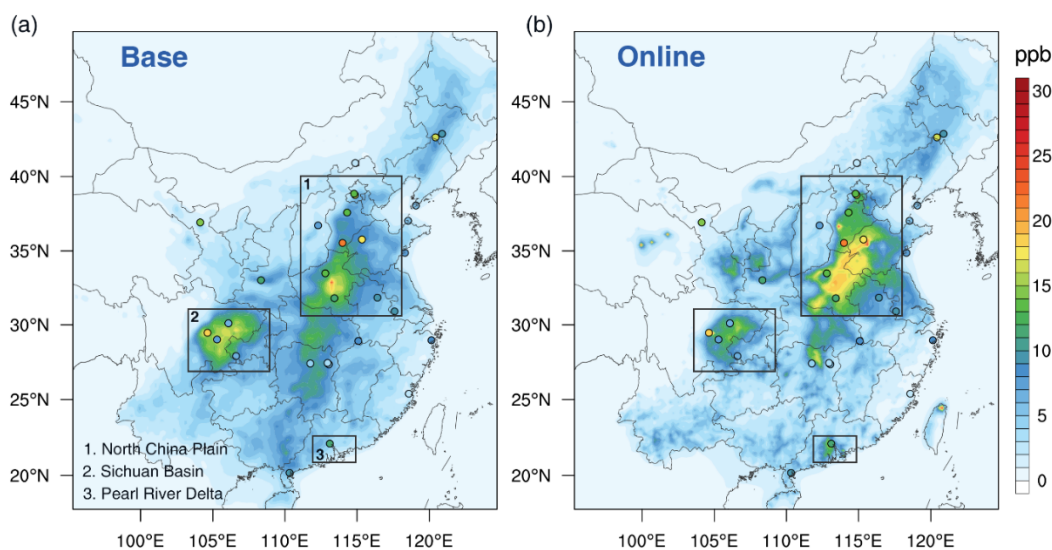
Figure 4: Spatial patterns of annual NH$_3$ concentrations over eastern China. The circles represent measured NH$_3$ concentration at Nationwide Nitrogen Deposition Monitoring Network (NNDMN) averaged for 2010-2015. The contour plots represent model NH$_3$ in 2019 from the base experiment (a) and online experiment (b) of this study. The black rectangles represent the three focused regions in eastern China.

350

Additionally, the Infrared Atmospheric Sounding Interferometer (IASI-A), launched aboard the European Space Agency's MetOpA in 2006, has observed atmospheric NH$_3$ at a global distribution and bi-daily resolution (09:30 and 21:30), here we use morning observations when the thermal contrast is more favourable for retrievals (Van Damme et al., 2014). The monthly NH$_3$ vertical column densities (VCDs) were determined based on the relative error weighting mean method (Van Damme et

355 al., 2014). The NH$_3$ VCDs from the simulations were calculated by integrating NH$_3$ molecular concentrations from the surface level to the top of the troposphere at 09:00 and 10:00 local time. As shown in Fig. 5, the online WRF-SoilN-Chem model was able to capture the general spatial distribution of NH$_3$ VCDs, including the higher concentrations over eastern China relative to western China, as well as the hot-spots over the NCP and the Sichuan Basin. As for temporal variation, monthly average NH$_3$ concentrations from online run compared to the IASI data showed similar seasonal cycles with highest concentrations in

360 summer, which is consistent with the time of agriculture activities and high ambient temperature. However, the online experiment slightly underestimated the NH$_3$ concentrations in spring (April) and winter (December) and a similar phenomenon was found by Li et al. (2021) and Liu et al. (2018). The difference between our model results and satellite observed distributions could be attributed to the uncertainty of NH$_3$ emission model and biases of satellite inversion algorithm. In satellite VCDs algorithm, the relative error weighting mean method always biases a high result due to the smaller relative error in a larger

365 column (Van Damme et al., 2014).
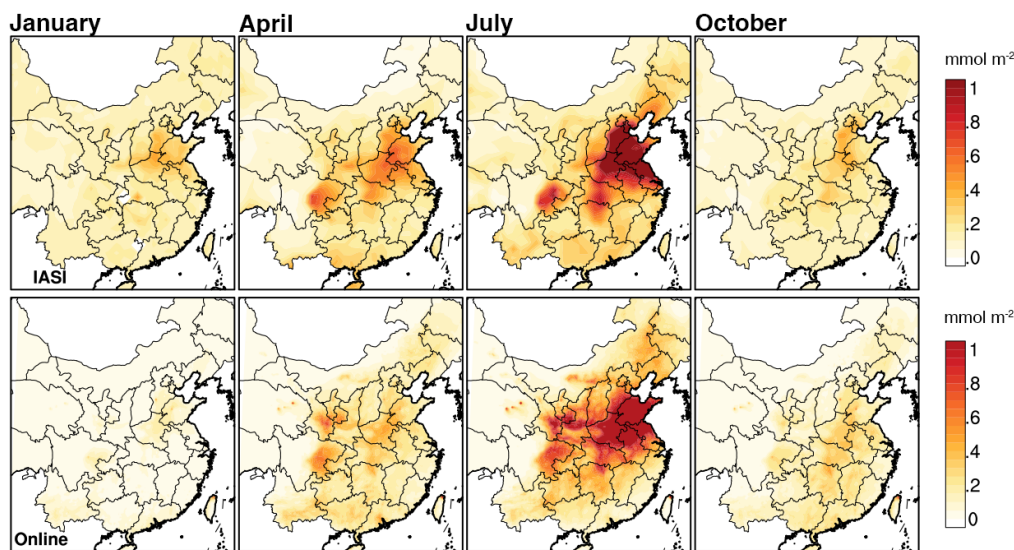
Figure 5: Comparison of column NH₃ concentrations between IASI satellite retrievals (upper panel), and WRF-Chem online (lower panel), averaged for January, April, July and October 2019.

3.4 Monthly variation of ammonia concentration and validation by in-situ observations

This newly-developed model in this work is capable of simulating varying NH_3 emission rate with changing climate, and monthly variations in the emission rate are compared with available observations. Figure 6 shows the monthly average of ground-site NH_3 with model results extracted at Nanjing and Beijing site locations. The observed NH_3 variations at two sites clearly demonstrated a minimum in winter and a maximum in summer that reflects the enhanced emission in growing season with higher temperature and denser fertilization. In the Nanjing site, the concentration of observed NH_3 ranged from 2.2 ppb in December to 23.0 ppb in July, with the annual average of 11.8 ppb. The small peak in April may be partly explained by the local seeding and fertilization of early rice. However, for base simulation, the NH_3 range was 0.02−14.26 ppb and the annual average was 4.99 ppb, which greatly underestimates NH_3 concentrations particularly for the warm season (e.g., May−September) (Fig. 6a). The base simulation NH_3 increases slightly from March to May, unable to reproduce the peak in April at all. Compared to the base run, the model with online flux shapes better seasonal variation, and the April-July averaged concentration has a similar magnitude as the observed NH_3 values (Fig. 6b). The interquartile ranges (shed width) are closer to the observations, and the proportion of overlaid area between observed and online shadows is reaching about 50 %, which is significantly larger than the base. Besides, the online experiment can capture the small peak in April with similar magnitude. For the Beijing site, the annual level of NH_3 is 14.2 ppb, which is higher than that in Nanjing site. This is consistent with the higher emission in the northern region than the southern region. The observed NH_3 concentration exhibits a large increase from 0.4 in January to 38.3 ppb in June. In contrast, the base simulated monthly ammonia concentration almost flat throughout

the whole year, which could not reproduce the observed significant seasonal variation at all. By comparison, online simulations notably narrowed the gap with observations, especially from March to September. The mean bias of NH$_3$ simulation was 10.5 and 8.2 ppb for the base and online experiments, respectively. However, for the winter seasons, from October to January, the online experiment overpredicts NH$_3$ at the Beijing site by an average of 95 %. This overestimation may be due to the meteorological or chemical simulation bias from WRF-Chem (Du et al., 2020; Liu et al., 2021) since both online and base experiments show overestimations of the Beijing site in winter.
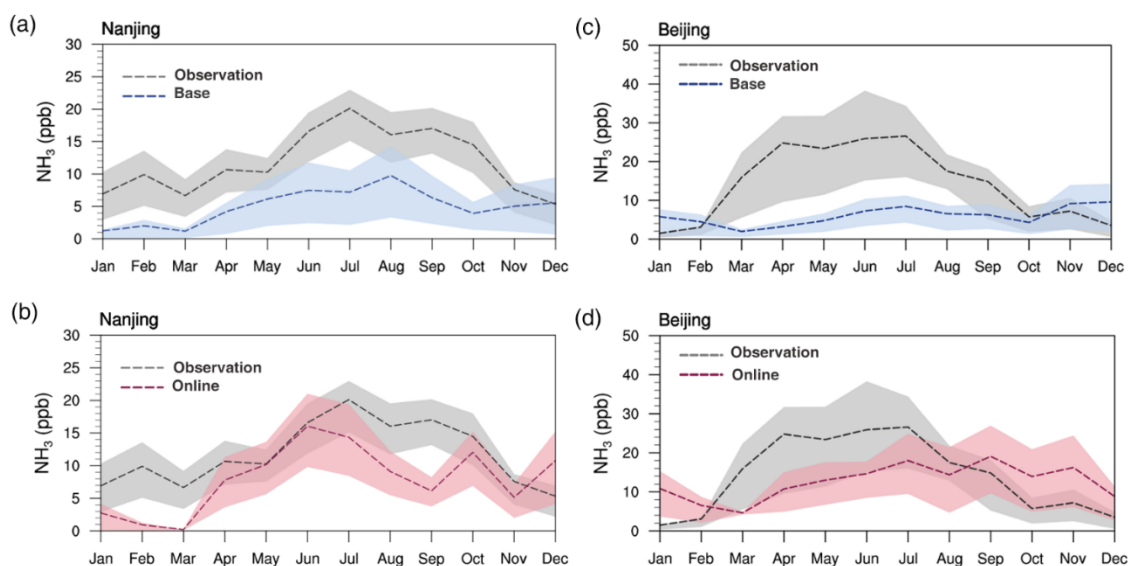
Figure 6: Monthly average ammonia concentrations at 2019 Nanjing site for base (a) and online (b) model runs and measurements from local. The dash lines indicate mean values. Lower and upper ends of the filled area indicate the 25th and 75th percentiles of each distribution. (c) and (d) are in Beijing site.

3.5 Comparison of hourly emission flux with field experiments

The most important advance of this model is the online calculation of highly time-resolved emission rate, available NH$_3$ emission flux at high temporal resolution was also collected to further validate the model. Air-surface exchanges of NH$_3$ were measured over a fertilized wheat canopy in the spring of 2012 in Hengshui, China. In the field, different plots of the cropland were cultivated by different farmers and the fertilization practices were conducted plot by plot. Ammonia flux measured from this kind of realistic cultivation conditions can represent real agriculture emission in the NCP. The NH$_3$ concentrations were continuously measured at two heights (2.5 m and 8 m) and Inverse Dispersion Method (IDM) was employed to derive the heterogeneous NH$_3$ emissions rate. Besides NH$_3$ flux, ancillary environment measurements of air temperature at 2 m, soil temperature at 0.05 m underground, wind speed and soil water content were also taken. The total input N for urea, nitrogen-

phosphorous-potassium and ammonium sulfate are averaged as 140 kg N ha^{-1}, 117 kg N ha^{-1} and 122 kg N ha^{-1}, respectively. The details of the measurement procedure were described in Huo et al. (2015).

The high temporal resolution variations of measured NH$_3$ flux and simulated flux are shown in Fig. 7. The mean observed and
410   modelled fluxes during this period were 22.3 mol km^{-2} hr^{-1} and 37.0 mol km^{-2} hr^{-1}, respectively. In Fig. 7(a), during 16th–17th October, the flux significantly decreased during the experiment for the duration of the rain. A similar tendency of low NH$_3$ flux during rainy days was found during observations, as reported from other studies (Osada, 2020; Roelle and Aneja, 2002). Increased contents of soil pore water dilute NH$_4^+$ in the liquid phase and inhibit its evaporation as NH$_3$. Furthermore, wet surfaces of cuticular leaves absorb ambient NH$_3$ under high relative humidity during rain. The model was able to reproduce
415   the low emission during the rain. In Fig. 7(b), the online dynamic model agrees well with diurnal field flux for the median values, while the 95th percentiles are much lower during daytime. The model captured the observed diurnal trends well with emission dominating during the day generally peaking at around the time of the maximum daily air temperature (12:00–14:00 local time). However, the model seemed to overestimate the measurements during the late morning when the measurements were dominated by deposition. Since the model only estimates unidirectional emission flux, the major deposition flux during
420   the 9:00–10:00 local time is not included in the model results, which leads to the overestimation of net emission flux by the model.
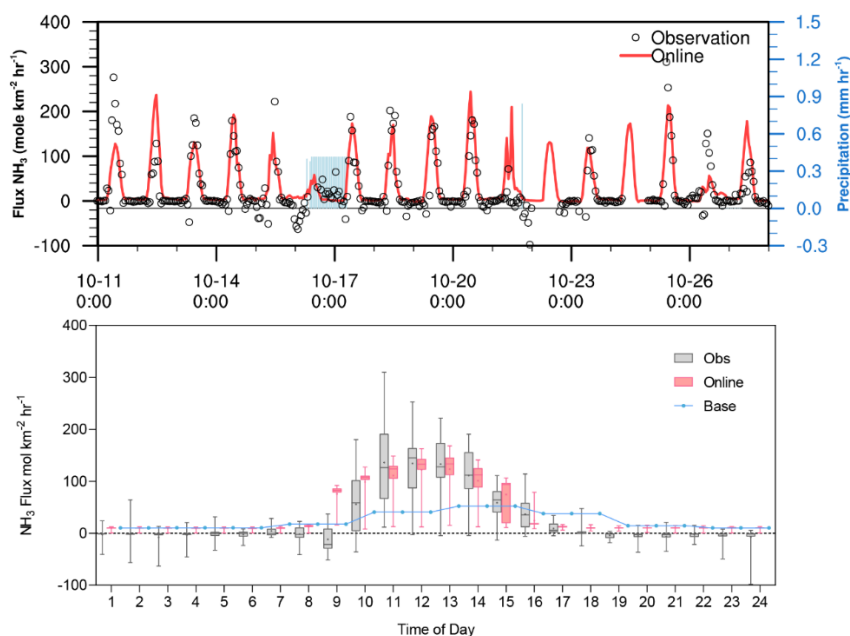
Figure 7: (a) Time series of observed (black symbol) and WRF-Chem Online model NH$_3$ flux (red line) above China Hengshui agri-field from the 11th to 27th October 2012. (b) Diel hourly box plots of observations flux measurements (grey), paired with online model results
425   (pink) and base model results (blue). The 5th and 95th percentiles are represented by the whiskers, the 25th and 75th quantiles are enclosed in

the box, the median is represented by the horizontal line through the box, and mean value is the dot in the box. Diurnal profile of emissions from agriculture is applied in base experiment following Du et al. (2020)

Due to weather change during the experiment, the diurnal NH_3 emission varied considerably with the large disparities between 5th and 95th percentiles, although at the same time of day. Despite the underestimation of the 5th percentiles, online emission results have obvious distribution with at least 25 % overlap with observation for each hour. However, fixed inventory used in the base simulation assumes no diurnal variation of emission. To integrate this inventory into WRF-Chem simulation, we adopted a diurnal profile with 80 % of NH_3 emissions in the daytime, following previous studies (Du et al., 2020). Obviously, the single line diurnal variation of the base experiment could not represent ammonia emission under real weather conditions.

3.6 Improved simulation of ammonia and secondary inorganic aerosol on synoptic scale

Once the gas ammonia is released into the atmosphere, some of them could actively participate in the atmospheric chemical reactions. As aforementioned, NH_3 is a very important alkaline constituent in the atmosphere and is a key precursor to the neutralization of gaseous sulfuric acid and gaseous nitric acid in the atmosphere to form the secondary inorganic aerosols, like sulfate, nitrate and ammonium, which contribute to ambient particulate matter. The amount that becomes aerosol ammonium (NH_4^+) depends on the concentrations of anions in the air, typically sulfate, nitrate, and chloride, which can form $(NH_4)_2SO_4$, NH_4HSO_4, NH_4NO_3, and ammonium chloride (NH_4Cl). Thus, an evaluation of ammonia flux would include both gas and aerosol forms ($NH_x = NH_3 + NH_4^+$). To investigate the response of NH_3 emission and aerosols to significant synoptic change, we choose two pronounced cases to evaluate the performance of the modified online model.

Figure 8(a) shows a typical case of NH_x episodes from 1st April to 8th April 2019 in Nanjing. There is a close association between the dramatic air temperature change and NH_x surface level. To be specific, NH_x concentration increased from 15 μg m^{-3} at air temperature below 10 °C to more than 30 μg m^{-3} at temperatures higher than 20 °C, suggesting a promotion effect of higher temperature to NH_3 emission and NH_x concentration in surface. Similar phenomena of a strong relationship between temperature and ammonia emission has also been proved by previous laboratory experiments (Clay et al., 1990; Pedersen et al., 2021; Niraula et al., 2018). Overall, the model with met-dependant mechanism well tracked the NH_x variation trends in observation period, and remarkably improved NH_x simulations with the MB decreasing from –9.5 to 0.7 μg m^{-3} in NH_x concentrations. Figure 8(b) shows the soil moisture and measured NH_x concentration variation from 1st to 18th January 2015 in Beijing site. In this case, the local NH_x concentration and soil moisture have similar variations with reaching peak together on 8th January and 15th January. The base simulation without considering soil moisture's effect significantly underestimates the NH_x peak concentration by ~30 μg m^{-3}. The online data can greatly capture the magnitude and temporal variation of NH_x concentration with the MB decreasing from –12.4 to –3.1 μg m^{-3}.

As the precursor gas, the performance of NH_3 simulation directly affects the formation of simulated secondary inorganic aerosols like NO_3^-. In Nanjing and Beijing, the base experiment shows nitrate aerosol was generally underestimated with MB of –5 μg m^{-3} due to the lack of NH_x (Fig. 9). The online model generally reproduced the observed nitrate concentration, with

a small mean bias from –4.5 to 1.9 μg m⁻³ in Nanjing case and from –5.2 to 0.8 μg m⁻³ in Beijing case. Comparison between

460   fixed emission input and online emission modelling clearly demonstrates that the numerical description of highly time-resolved

NH₃ emission has a superior performance on the magnitude and temporal variation of secondary aerosol.
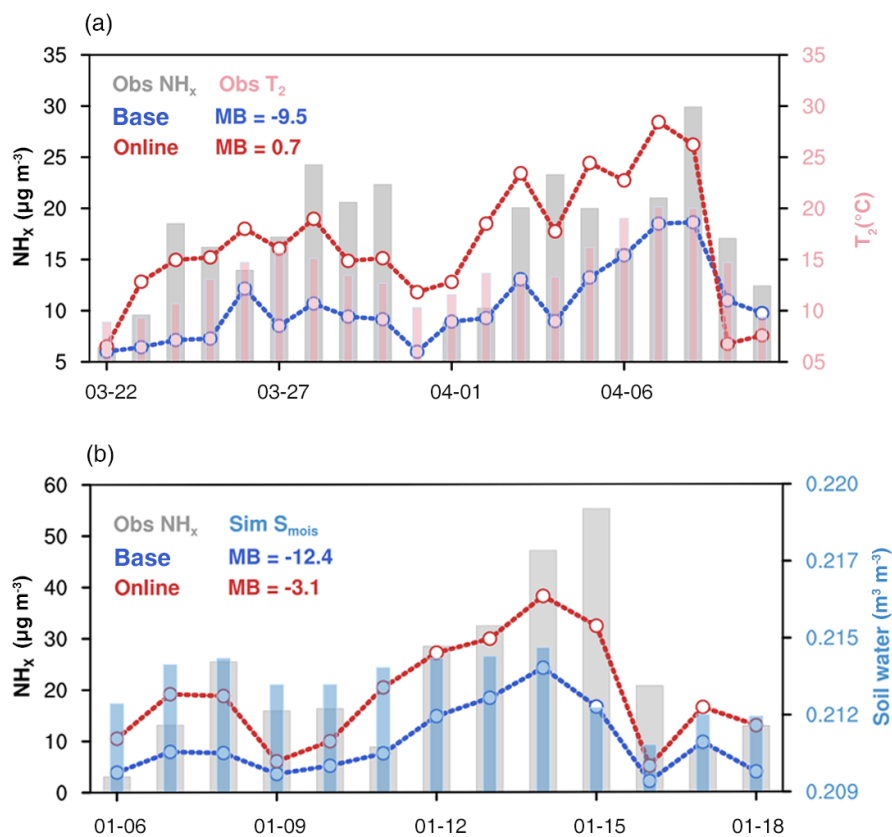
Figure 8: (a) Time series of total ammonia (NH$_x$) concentrations from 22nd March to 11th April 2019 in Nanjing site. The T$_2$ represents the air temperature at 2m ground level from local site. (b) Time series of NH$_x$ concentrations from 6th to 18th January 2015 in Beijing site. S$_{mois}$

465   represents the top 5cm thick layer soil water which is derived from WRF model calculations. The mean bias of modelled concentrations is

labelled by MB.
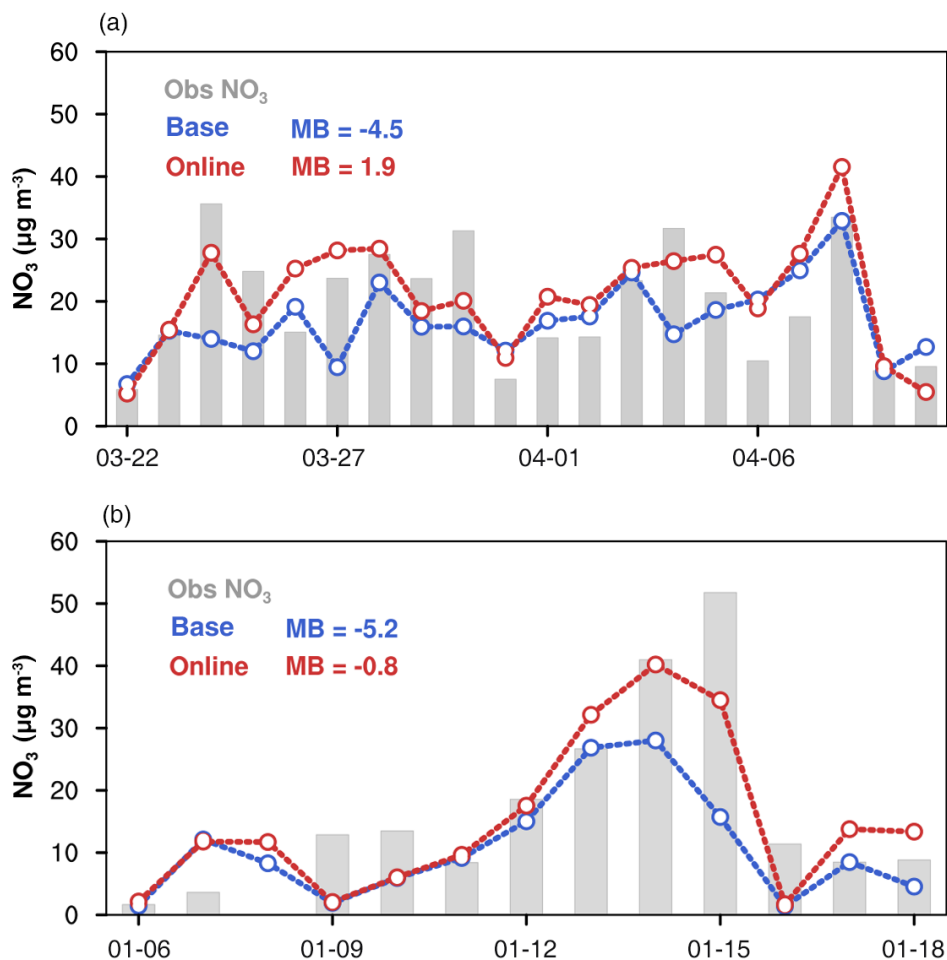
Figure 9: (a) Time series of nitrate (NO$_3^-$) concentrations from 22nd March to 11th April 2019 in Nanjing site. (b) Time series of nitrate (NO$_3^-$) concentrations from 6th – 18th January 2015 in Beijing site.

4 Summary and Future work

We developed the WRF-SoilN-Chem (v1.0) model, which is an online coupling of the WRF meteorological model and dynamic NH$_3$ flux model, to simulate meteorology-dependent regional NH$_3$ emission at high spatiotemporal resolution. In this model, high resolution basic emission data and meteorology-dependant parameterizations were implemented, and soil temperature, wind speed, soil moisture and rainfall simulated from WRF were considered as the important factor in the parametrization to control NH$_3$ emission. This version can be easily implemented in other regional or global models and could serve as a tool for more precise and highly time-resolved estimation of the NH$_3$ emission calculations.

The preliminary evaluation by multiple ground-based and satellite observations indicates that the WRF-SoilN-Chem model is able to better represent the spatiotemporal variation of surface NH_3 concentrations over eastern China than the widely used offline MEIC NH_3 inventory. We evaluated the model by field experimental data, monitor observation and satellite retrievals. Compared to the monthly offline inventory, this simple model well reproduced the diurnal variation of NH_3 flux measured in the typical farmland. Our first application showed that the WRF-SoilN-Chem model was able to capture the magnitude spatiotemporal variation of NH_3 surface and column concentrations over China in 2019. And this model has smaller biases in the simulation of ammonia at both Beijing and Nanjing monitoring stations. The seasonal variations from the online calculation in WRF-SoilN-Chem model are distinct and have similar patterns as observations which are characterized by high concentrations in summer and low concentrations in winter.

The consideration of meteorological factors makes the model more accurate for ammonia simulations under conditions of drastic weather changes. To be specific, the mean bias of NH_x simulation during Nanjing and Beijing case period were −9.5 and −12.4 μg m^{-3} without the influence of dynamic meteorological factor, reducing to 0.7 and −3.1 μg m^{-3} when considering temperature and soil moisture's effect. Besides, higher and precise NH_x concentration favors the formation of nitrate by enhancing gas-particle conversion, reducing the mean bias of nitrate concentration from –4.5 to 1.9 and from −5.2 to −0.8 μg m^{-3} in Nanjing and Beijing, respectively. In general, with the met-dependence mechanism, the online model can optimize the simulation of surface NH_x and NO_3^- under dynamically changing weather.

Despite providing more accurate and high-resolution estimation of NH_3 emission, the current version of the WRF-SoilN-Chem (version 1.0) still has some limitations and needs further improvements, including (1) the option to use bidirectional NH_3 flux model based on a resistance approach; (2) update of the dynamic emission factor parameterization with more field experiment results; (3) development of soil emission modules for other atmospherically reactive species, such as HONO and NOx. Such improvements could make the WRF-SoilN-Chem an increasingly useful tool to analyse NH_3 emission and its impact on air pollution and biogeochemical nitrogen cycling.

Code and data availability

NH_3 vertical column density data are freely available through the AERIS database: https://iasi.aeris-data.fr/NH3/. The Nationwide Nitrogen Deposition Monitoring Network data are publicly available at https://doi.org/10.1038/s41597-019-0061-2. The standard WRF-Chem v3.9 is freely accessible to the public by following https://github.com/wrf-model/WRF/releases. The source codes of dynamic NH_3 emission model and input files about basic emission file presented in the article have been archived and made publicly available for downloading from https://doi.org/10.5281/zenodo.7134286.

Author contributions

XH, YS and TZ conceived the idea and guided the study. CR and XH did model construction, simulations, and paper writing. YS provided the field experiment and flux measurement. XL and ZW provided NNDMN monitoring data of ammonia

510   concentration. All authors contributed to the writing and editing of this paper.

Competing interests

The authors declare that they have no conflict of interest.

Financial support

This work was supported by National Natural Science Foundation of China (41875150 and 41922038), and the Fundamental

515   Research Funds for the Central Universities (14380187).

Reference

Asman, W. A. H.: Modelling the atmospheric transport and deposition of ammonia and ammonium: an overview with special
        reference to Denmark, Atmos. Environ., 35, 1969-1983, https://doi.org/10.1016/S1352-2310(00)00548-3, 2001.

Behera, S. N., Sharma, M., Aneja, V. P., and Balasubramanian, R.: Ammonia in the atmosphere: a review on emission sources,

520   atmospheric chemistry and deposition on terrestrial bodies, Environ. Sci. Pollut. R., 20, 8092-8131,
        https://doi.org/10.1007/s11356-013-2051-9, 2013.

Bouwman, A. F., Boumans, L. J. M., and Batjes, N. H.: Estimation of global NH3 volatilization loss from synthetic fertilizers
        and   animal   manure   applied   to   arable   lands   and   grasslands,   Global   Biogeochem.   Cy.,   16,
        https://doi.org/10.1029/2000gb001389, 2002.

525 Bouwman, A. F., Lee, D. S., Asman, W. A. H., Dentener, F. J., VanderHoek, K. W., and Olivier, J. G. J.: A global high-
        resolution emission inventory for ammonia, Global Biogeochem. Cy., 11, 561-587, https://doi.org/10.1029/97gb02266,
        1997.

Chen, D., Liu, Z. Q., Fast, J., and Ban, J. M.: Simulations of sulfate-nitrate-ammonium (SNA) aerosols during the extreme
        haze events over northern China in October 2014, Atmos. Chem. Phys., 16, 10707-10724, https://doi.org/10.5194/acp-

530   16-10707-2016, 2016.

Clay, D. E., Malzer, G. L., and Anderson, J. L.: Ammonia volatilization from urea as influenced by soil-temperature, soil-
        water   content,   and   nitrification   and   hydrolysis   inhibitors,   Soil.   Sci.   Soc.   Am.   J.,   54,   263-266,
        https://doi.org/10.2136/sssaj1990.03615995005400010042x, 1990.

Cooter, E. J., Bash, J. O., Walker, J. T., Jones, M. R., and Robarge, W.: Estimation of NH3 bi-directional flux from managed agricultural soils, Atmos. Environ., 44, 2107-2115, https://doi.org/ 10.1016/j.atmosenv.2010.02.044, 2010.

Crippa, M., Solazzo, E., Huang, G. L., Guizzardi, D., Koffi, E., Muntean, M., Schieberle, C., Friedrich, R., and Janssens-Maenhout, G.: High resolution temporal profiles in the emissions database for global atmospheric research, Sci. Data, 7, https://doi.org/10.1038/s41597-020-0462-2, 2020.

Denmead, O. T., Freney, J. R., and Simpson, J. R.: Dynamics of Ammonia Volatilization during Furrow Irrigation of Maize, Soil. Sci. Soc. Am. J., 46, 149-155, https://doi.org/10.2136/sssaj1982.03615995004600010028x, 1982.

Ding, A., Huang, X., and Fu, C.: Air Pollution and Weather Interaction in East Asia, https://doi.org/10.1093/acrefore/9780199389414.013.536, 2017.

Du, Q. Y., Zhao, C., Zhang, M. S., Dong, X., Chen, Y., Liu, Z., Hu, Z. Y., Zhang, Q., Li, Y. B., Yuan, R. M., and Miao, S. G.: Modeling diurnal variation of surface PM2.5 concentrations over East China with WRF-Chem: impacts from boundary-layer mixing and anthropogenic emission, Atmos. Chem. Phys., 20, 2839-2863, https://doi.org/10.5194/acp-20-2839-2020, 2020.

Ek, M. B., Mitchell, K. E., Lin, Y., Rogers, E., Grunmann, P., Koren, V., Gayno, G., and Tarpley, J. D.: Implementation of Noah land surface model advances in the National Centers for Environmental Prediction operational mesoscale Eta model, J. Geophys. Res. Atmos., 108, https://doi.org/10.1029/2002jd003296, 2003.

Emmanouil, C., Drositi, E., Vasilatou, V., Diapouli, E., Krikonis, K., Eleftheriadis, K., and Kungolos, A.: Study on particulate matter air pollution, source origin, and human health risk based of PM10 metal content in Volos City, Greece, Toxicol. Environ. Chem., 99, 691-709, https://doi.org/10.1080/02772248.2016.1242005, 2017.

Fenn, L. B. and Kissel, D. E.: The Influence of Cation Exchange Capacity and Depth of Incorporation on Ammonia Volatilization from Ammonium Compounds Applied to Calcareous Soils, Soil Sci. Soc. Am. J., 40, 394-398, https://doi.org/ https://doi.org/10.2136/sssaj1976.03615995004000030026x, 1976.

Ferguson, R. B. and Kissel, D. E.: Effects of Soil Drying on Ammonia Volatilization from Surface-applied Urea, Soil Sci. Soc. Am. J., 50, 485-490, https://doi.org/ https://doi.org/10.2136/sssaj1986.03615995005000020047x, 1986.

Fowler, D., Coyle, M., Skiba, U., Sutton, M. A., Cape, J. N., Reis, S., Sheppard, L. J., Jenkins, A., Grizzetti, B., Galloway, J. N., Vitousek, P., Leach, A., Bouwman, A. F., Butterbach-Bahl, K., Dentener, F., Stevenson, D., Amann, M., and Voss, M.: The global nitrogen cycle in the twenty-first century, Philos. Trans. R. Soc. Lond., B, Biol. Sci., 368, 20130164, https://doi.org/10.1098/rstb.2013.0164, 2013.

Grell, G. A. and Freitas, S. R.: A scale and aerosol aware stochastic convective parameterization for weather and air quality modeling, Atmos. Chem. Phys., 14, 5233-5250, https://doi.org/10.5194/acp-14-5233-2014, 2014.

Grell, G. A., Peckham, S. E., Schmitz, R., McKeen, S. A., Frost, G., Skamarock, W. C., and Eder, B.: Fully coupled "online" chemistry within the WRF model, Atmos. Environ., 39, 6957-6975, https://doi.org/10.1016/j.atmosenv.2005.04.027, 2005.

Gyldenkaerne, S., Skjoth, C. A., Hertel, O., and Ellermann, T.: A dynamical ammonia emission parameterization for use in air pollution models, J. Geophys. Res. Atmos., 110, https://doi.org/10.1029/2004jd005459, 2005.

Hong, S. Y., Noh, Y., and Dudhia, J.: A new vertical diffusion package with an explicit treatment of entrainment processes, Mon. Weather. Rev., 134, 2318-2341, https://doi.org/10.1175/Mwr3199.1, 2006.

Huang, X., Song, Y., Li, M. M., Li, J. F., Huo, Q., Cai, X. H., Zhu, T., Hu, M., and Zhang, H. S.: A high-resolution ammonia emission inventory in China, Global Biogeochem. Cy., 26, https://doi.org/10.1029/2011gb004161, 2012.

Huo, Q., Cai, X. H., Kang, L., Zhang, H. S., Song, Y., and Zhu, T.: Estimating ammonia emissions from a winter wheat cropland in North China Plain with field experiments and inverse dispersion modeling, Atmos. Environ., 104, 1-10, https://doi.org/10.1016/j.atmosenv.2015.01.003, 2015.

Iacono, M. J., Delamere, J. S., Mlawer, E. J., Shephard, M. W., Clough, S. A., and Collins, W. D.: Radiative forcing by long-lived greenhouse gases: Calculations with the AER radiative transfer models, J. Geophys. Res. Atmos., 113, https://doi.org/10.1029/2008jd009944, 2008.

Kong, L., Tang, X., Zhu, J., Wang, Z. F., Pan, Y. P., Wu, H. J., Wu, L., Wu, Q. Z., He, Y. X., Tian, S. L., Xie, Y. Z., Liu, Z. R., Sui, W. X., Han, L. N., and Carmichael, G.: Improved Inversion of Monthly Ammonia Emissions in China Based on the Chinese Ammonia Monitoring Network and Ensemble Kalman Filter, Environ. Sci. Technol., 53, 12529-12538, https://doi.org/10.1021/acs.est.9b02701, 2019.

Kurokawa, J. and Ohara, T.: Long-term historical trends in air pollutant emissions in Asia: Regional Emission inventory in ASia (REAS) version 3, Atmos. Chem. Phys., 20, 12761-12793, https://doi.org/10.5194/acp-20-12761-2020, 2020.

Li, B., Chen, L., Shen, W., Jin, J., Wang, T., Wang, P., Yang, Y., and Liao, H.: Improved gridded ammonia emission inventory in China, Atmos. Chem. Phys., 21, 15883-15900, https://doi.org/10.5194/acp-21-15883-2021, 2021.

Li, M., Liu, H., Geng, G. N., Hong, C. P., Liu, F., Song, Y., Tong, D., Zheng, B., Cui, H. Y., Man, H. Y., Zhang, Q., and He, K. B.: Anthropogenic emission inventories in China: a review, Natl. Sci. Rev., 4, 834-866, https://doi.org/10.1093/nsr/nwx150, 2017.

Lian, Z. M., Ouyang, W., Liu, H. B., Zhang, D., and Liu, L. H.: Ammonia volatilization modeling optimization for rice watersheds under climatic differences, Sci. Total Environ., 767, https://doi.org/10.1016/j.scitotenv.2020.144710, 2021.

Lin, Y. L., Farley, R. D., and Orville, H. D.: Bulk Parameterization of the Snow Field in a Cloud Model, J. Appl. Meteorol. Climatol., 22, 1065-1092, https://doi.org/10.1175/1520-0450(1983)022<1065:Bpotsf>2.0.Co;2, 1983.

Liu, C., Huang, J. P., Hu, X. M., Hu, C., Wang, Y. W., Fang, X. Z., Luo, L., Xiao, H. W., and Xiao, H. Y.: Evaluation of WRF-Chem simulations on vertical profiles of PM2.5 with UAV observations during a haze pollution event, Atmos. Environ., 252, 118332, https://doi.org/10.1016/j.atmosenv.2021.118332, 2021.

Liu, F., Sun, F. B., Liu, W. W., Wang, T. T., Wang, H., Wang, X. M., and Lim, W. H.: On wind speed pattern and energy potential in China, Appl. Energy, 236, 867-876, https://doi.org/10.1016/j.apenergy.2018.12.056, 2019.

Liu, L., Xu, W., Lu, X. K., Zhong, B. Q., Guo, Y. X., Lu, X., Zhao, Y. H., He, W., Wang, S. H., Zhang, X. Y., Liu, X. J.,
Vitousek, P.: Exploring global changes in agricultural ammonia emissions and their contribution to nitrogen deposition
since 1980, Proc. Natl. Acad. Sci. U.S.A., 119, e2121998119, https://doi.org/10.1073/pnas.2121998119, 2022.

Liu, M. X., Huang, X., Song, Y., Xu, T. T., Wang, S. X., Wu, Z. J., Hu, M., Zhang, L., Zhang, Q., Pan, Y. P., Liu, X. J., and
Zhu, T.: Rapid SO2 emission reductions significantly increase tropospheric ammonia concentrations over the North China
Plain, Atmos. Chem. Phys., 18, 17933-17943, https://doi.org/10.5194/acp-18-17933-2018, 2018.

Longhini, V. Z., Cardoso, A. D., Berca, A. S., Boddey, R. M., Reis, R. A., Dubeux, J. C. B., and Ruggieri, A. C.: Nitrogen
supply and rainfall affect ammonia emissions from dairy cattle excreta and urea applied on warm-climate pastures, J.
Environ. Qual, 49, 1453-1466, https://doi.org/10.1002/jeq2.20167, 2020.

Maru, A., Haruna, A., Majid, N., Charles Primus, W., Maikol, N., Asap, A., Naharuddin, A., and Jeffary, A.: Using Soil Water
to Control Ammonia Emission from Acid Soils with and Without Chicken Litter Biochar, Sustain. Environ. Res., 8, 23,
https://doi.org/10.5539/sar.v8n3p23, 2019.

Mcinnes, K. J., Ferguson, R. B., Kissel, D. E., and Kanemasu, E. T.: Ammonia Loss from Applications of Urea Ammonium-
Nitrate Solution to Straw Residue, Soil Sci. Soc. Am. J., 50, 969-974,
https://doi.org/10.2136/sssaj1986.03615995005000040028x, 1986.

Misselbrook, T. H., Nicholson, F. A., Chambers, B. J., and Johnson, R. A.: Measuring ammonia emissions from land applied
manure: an intercomparison of commonly used samplers and techniques, Environ. Pollut., 135, 389-397,
https://doi.org/10.1016/j.envpol.2004.11.012, 2005.

Niraula, S., Rahman, S., and Chatterjee, A.: Temperature response of ammonia and greenhouse gas emission from manure
amended silty clay soil, Acta Agric. Scand. B Soil. Plant. Sci., 68, 663-677,
https://doi.org/10.1080/09064710.2018.1459822, 2018.

Oprea, M., Dunea, D., and Liu, H. Y.: Development of a Knowledge Based System for Analyzing Particulate Matter Air
Pollution Effects on Human Health, Environ. Eng. Manag. J., 16, 669-676, https://doi.org/10.30638/eemj.2017.068, 2017.

Osada, K.: Measurement report: Short-term variation in ammonia concentrations in an urban area increased by mist
evaporation and emissions from a forest canopy with bird droppings, Atmos. Chem. Phys., 20, 11941-11954,
https://doi.org/10.5194/acp-20-11941-2020, 2020.

Overrein, L. N. and Moe, P. G.: Factors Affecting Urea Hydrolysis and Ammonia Volatilization in Soil, Soil. Sci. Soc. Am.
J., 31, 57-&, https://doi.org/10.2136/sssaj1967.03615995003100010018x, 1967.

Paerl, H. W.: Connecting atmospheric nitrogen deposition to coastal eutrophication, Environ. Sci. Technol., 36, 323a-326a,
https://doi.org/10.1021/es022392a, 2002.

Parker, D. B., Pandrangi, S., Greene, L. W., Almas, L. K., Cole, N. A., Rhoades, A. B., and Koziel, J. A.: Rate and frequency
of urease inhibitor application for minimizing ammonia emissions from beef cattle feedyards, Trans. ASAE, 48, 787-793,
2005.

Paulot, F., Jacob, D. J., Pinder, R. W., Bash, J. O., Travis, K., and Henze, D. K.: Ammonia emissions in the United States, European Union, and China derived by high-resolution inversion of ammonium wet deposition data: Interpretation with a new agricultural emissions inventory (MASAGE_NH3), J. Geophys. Res. Atmos., 119, 4343-4364, https://doi.org/10.1002/2013jd021130, 2014.

Pedersen, J., Nyord, T., Feilberg, A., and Labouriau, R.: Analysis of the effect of air temperature on ammonia emission from band application of slurry, Environ. Pollut., 282, https://doi.org/10.1016/j.envpol.2021.117055, 2021.

Pleim, J. E., Ran, L., Appel, W., Shephard, M. W., and Cady-Pereira, K.: New bidirectional ammonia flux model in an air quality model coupled with an agricultural model, J. Adv. Model. Earth Syst., 11, 2934-2957, https://doi.org/10.1029/2019MS001728, 2019.

Riddick, S., Ward, D., Hess, P., Mahowald, N., Massad, R., and Holland, E.: Estimate of changes in agricultural terrestrial nitrogen pathways and ammonia emissions from 1850 to present in the Community Earth System Model, Biogeosciences, 13, 3397-3426, https://doi.org/10.5194/bg-13-3397-2016, 2016.

Roelle, P. A. and Aneja, V. P.: Characterization of ammonia emissions from soils in the upper coastal plain, North Carolina, Atmos. Environ., 36, 1087-1097, https://doi.org/10.1016/S1352-2310(01)00355-7, 2002.

Ryan, J., Curtin, D., and Safi, I.: Ammonia Volatilization as Influenced by Calcium-Carbonate Particle-Size and Iron-Oxides, Soil. Sci. Soc. Am. J., 45, 338-341, https://doi.org/10.2136/sssaj1981.03615995004500020022x, 1981.

Sanz-Cobena, A., Misselbrook, T., Camp, V., and Vallejo, A.: Effect of water addition and the urease inhibitor NBPT on the abatement of ammonia emission from surface applied urea, Atmos. Environ., 45, 1517-1524, https://doi.org/10.1016/j.atmosenv.2010.12.051, 2011.

Skamarock, W. C.: A Discription of the Advanced Research WRF model Version 4, 2019.

Smith, C. J., Freney, J. R., Chalk, P. M., Galbally, I. E., Mckenney, D. J., and Cai, G. X.: Fate of Urea Nitrogen Applied in Solution in Furrows to Sunflowers Growing on a Red-Brown Earth - Transformations, Losses and Plant Uptake, Aust. J. Agric. Resour. Econ., 39, 793-806, https://doi.org/10.1071/Ar9880793, 1988.

Smith, E., Gordon, R., Bourque, C., Campbell, A., Genermont, S., Rochette, P., and Mkhabela, M.: Simulated management effects on ammonia emissions from field applied manure, J. Environ. Manage, 90, 2531-2536, https://doi.org/10.1016/j.jenvman.2009.01.012, 2009.

Sommer, S. G., Olesen, J. E., and Christensen, B. T.: Effects of temperature, wind speed and air humidity on ammonia volatilization from surface applied cattle slurry, J. Agric. Sci., 117, 91-100, https://doi.org/10.1017/s0021859600079016, 1991.

Spindler, G., Teichmann, U., and Sutton, M. A.: Ammonia dry deposition over grassland - micrometeorological flux-gradient measurements and bidirectional flux calculations using an inferential model, Q. J. R. Meteorol. Soc., 127, 795-814, https://doi.org/ doi:10.1002/qj.49712757305, 2001.

U.S. EPA, https://www.tceq.texas.gov/downloads/meteorological-model-performance-evaluation-for-2019, 2021.

665   Van Damme, M., Erisman, J. W., Clarisse, L., Dammers, E., Whitburn, S., Clerbaux, C., Dolman, A. J., and Coheur, P. F.:
         Worldwide spatiotemporal atmospheric ammonia (NH3) columns variability revealed by satellite, Geophys. Res. Lett,
         42, 8660-8668, https://doi.org/10.1002/2015gl065496, 2015.

        Van Damme, M., Clarisse, L., Heald, C. L., Hurtmans, D., Ngadi, Y., Clerbaux, C., Dolman, A. J., Erisman, J. W., and Coheur,
         P. F.: Global distributions, time series and error characterization of atmospheric ammonia (NH3) from IASI satellite
670   observations, Atmos. Chem. Phys., 14, 2905-2922, https://doi.org/10.5194/acp-14-2905-2014, 2014.

        van Pul, A., Reis, S., Dore, T., Liu, X. J., Fagerli, H., Geels, C., Hertel, O., Kruijt, R. W., Kryza, M., Bergstrom, R., Vieno,
         M., Smith, R., and Nemitz, E.: Modelling the National and Regional Transport and Deposition of Ammonia, Atmospheric
         Ammonia, 409-+, https://doi.org/10.1007/978-1-4020-9121-6_25, 2009.

        Van Slyke, D. D. and Cullen, G. E.: The mode of action of urease and of enzymes in general., J. Biol. Chem., 19, 141-180,
675   https://doi.org/10.1016/S0021-9258(18)88300-4, 1914.

        Wang, Y., Zhang, Q. Q., He, K., Zhang, Q., and Chai, L.: Sulfate-nitrate-ammonium aerosols over China: response to 2000-
         2015 emission changes of sulfur dioxide, nitrogen oxides, and ammonia, Atmos. Chem. Phys., 13, 2635-2652,
         https://doi.org/10.5194/acp-13-2635-2013, 2013.

        Webb, J. and Misselbrook, T. H.: A mass-flow model of ammonia emissions from UK livestock production, Atmos. Environ.,
680   38, 2163-2176, https://doi.org/10.1016/j.atmosenv.2004.01.023, 2004.

        Webb, J., Ryan, M., Anthony, S. G., Brewer, A., Laws, J., Aller, M. F., and Misselbrook, T. H.: Cost-effective means of
         reducing ammonia emissions from UK agriculture using the NARSES model, Atmos. Environ., 40, 7222-7233,
         https://doi.org/10.1016/j.atmosenv.2006.06.029, 2006.

        Xu, W., Zhang, L., and Liu, X. J.: A database of atmospheric nitrogen concentration and deposition from the nationwide
685   monitoring network in China, Sci. Data, 6, https://doi.org/10.1038/s41597-019-0061-2, 2019.

        Zaveri, R. A. and Peters, L. K.: A new lumped structure photochemical mechanism for large-scale applications, J. Geophys.
         Res. Atmos., 104, 30387-30415, https://doi.org/ 10.1029/1999jd900876, 1999.

        Zaveri, R. A., Easter, R. C., Fast, J. D., and Peters, L. K.: Model for Simulating Aerosol Interactions and Chemistry (MOSAIC),
         J. Geophys. Res. Atmos., 113, https://doi.org/10.1029/2007jd008782, 2008.

690   Zhang, L., Wright, L. P., and Asman, W. A. H.: Bi-directional air-surface exchange of atmospheric ammonia: A review of
         measurements and a development of a big-leaf model for applications in regional-scale air-quality models, J. Geophys.
         Res. Atmos., 115, https://doi.org/10.1029/2009jd013589, 2010a.

        Zhang, T. Y., Li, T., Yue, X., and Yang, X. G.: Impacts of aerosol pollutant mitigation on lowland rice yields in China, Environ.
         Res. Lett., 12, https://doi.org/10.1088/1748-9326/aa80f0, 2017.

695   Zhang, Y., Dore, A. J., Ma, L., Liu, X. J., Ma, W. Q., Cape, J. N., and Zhang, F. S.: Agricultural ammonia emissions inventory
         and   spatial   distribution   in   the   North   China   Plain,   Environ.   Pollut.,   158,   490-501,
         https://doi.org/10.1016/j.envpol.2009.08.033, 2010b.

Zheng, X. J., Yu, Z. W., Zhang, Y. L., and Shi, Y.: Effect of nitrogen rates on wheat photosynthesis, anatomical parameters and photoassimilate partitioning in North China Plain, Int. J. Plant. Prod., 15, 161-172, https://doi.org/10.1007/s42106-
700   020-00123-3, 2021.